Strong Light Confinement and High Absorption of Metal-Dielectric-Metal(MDM) Cylindrical Microcavities

Heng Hang

(Analysis and Testing Center,Nanjing Normal University,Nanjing 210023,China)

Abstract:Plasmonic nanostructures concentrate optical field into extremely tiny volumes, which is useful for surface enhanced spectroscopy, bio-sensing and solar cells. We present the design of a cylindrical microcavity of high absorption and strong light confinement. The cylindrical microcavity is based on Au-dielectric-Au sandwiched structure. Numerically study shows that cylindrical microcavity can provide high electromagnetic average energy density and contain the most energy of the incoming light. The enhancement factor of average energy density G is up to $10^3 \sim 10^4$-fold inside the cavity. The calculation results show that the G presents the regularities with the change of the thickness of the dielectric slab, dielectric constant and the radius of gold disk. At the normal incidence of electromagnetic radiation, the obtained reflection spectra operate in the range from 4.8 μm to 6 μm and the absorption efficiency $C(C = 1-R_{min})$ reaches 99% by optimizing the dielectric constant and the structure's geometry parameters.

Key words:microcavity,metal-semiconductor-metal,absorption

基于金属-介质-金属圆柱体微腔的光的强局域和高吸收特性

衡　航

(南京师范大学分析测试中心,江苏 南京 210023)

[**摘要**]　等离激元纳米结构能够把光场局域到非常小的空间,而应用在表面增强光谱、生物传感和太阳能电池等领域. 我们设计了一种对光场具有高局域和强吸收特性的基于金-介质-金三明治结构的圆柱体微腔结构. 计算结果显示:该圆柱微腔能够局域入射光的绝大部分能量,产生强的平均电磁场能量密度. 微腔内的平均电磁场能量密度增强因子 G 达到 $10^3 \sim 10^4$ 数量级,而且 G 值随着介质层的厚度、介电常数和圆饼半径的变化呈现出了一定的变化规律. 在正入射波的条件下,经计算得到了 4.8 μm~6 μm 范围的反射光谱和吸收率 $C(C = 1-R_{min})$,通过优化介电常数和结构的几何参数,C 值达到 99%.

[**关键词**]　微腔,金属-半导体-金属,吸收

Surface plasmon polaritons(SPPs) and localized surface plasmon polaritons(LSPs) have become an important theoretical basis in the field of optical metamaterials[1]. Metal-dielectric structures[2] are usually used to excite SPPs and LSPs. At the normal incidence of electromagnetic radiation, the penetration depth into dielectric layer deepens with the wavelength increase in the infrared range. At the same time, the Ohmic loss of metal layers reduces reversely[3]. Particularly in the far infrared, the Ohmic loss is very close to zero and metal layer has a perfect reflection characteristic. So we can break the diffraction limit and confine light within the dielectric layer[4]. In terahertz, dimensions can be reduced to extremely subwavelength[5]. Further more, Fevillet-Palma et al[6] have

studied the near-field enhancement properties of the antenna in the terahertz and originally calculated the electro-magnetic energy density in the cavities. However, the cuboid microcavities have lower absorption efficiency. And this cuboids cavity is sensitive to the polarization of the incident wave.

In this work, we firstly proposed a metal-dielectric-metal(MDM) cylindrical microcavities and numerically calculated the electromagnetic energy density in the cavities, the concentration mechanism and absorption properties of the cylindrical microcavities through mathematical model by HFSS(High Frequency Structure Simulator, Commercial Software). Compared with the literature[6], we got higher absorption efficiency C. Due to the gold disk being of circular symmetry, the structure is insensitive to polarization of the incident light. The proposed model and calculation method will play guidance role in the optimization of substrates for surface enhanced spectroscopy.

1 Structures and Methods

The designed MDM structure is simulated by HFSS, a finite element method based program. The MDM cylindrical cavities are periodically arranged in a square lattice in the $X-Y$ plane, as shown in the Fig. 1(a). Fig. 1(b) is the schematic of a unit cell of the cylindrical cavity array. A dielectric layer is sandwiched between two metallic layers, the top layer is gold disk and the bottom layer is gold ground layer. The red area in Fig. 1(b) is the cylindrical microcavity formed between a gold disk and a gold ground layer. If the dielectric layer thickness L is smaller than the wavelength, such structure supports a TM_{100} mode[6]. Fig. 1(c) shows the cross section of the cavity in the $Y-Z$ plane, and the structural parameters are shown in the figure. The thickness of the dielectric layer is chosen as L, h and r are defined as the thickness and radius of the gold disk, respectively. In this work, the thickness of the gold ground layer is chosen as 0.45 μm. The gold ground layer has two significant functions. One is to serve as an optical mirror. As the thickness is greater than the penetration depth of the incident light, the transmittance is close to zero. The other is to couple with the gold disk and gold ground layer to create electric and magnetic dipoles which extremely concentrate electromagnetic energy into the microcavities. Period P is 3 μm. The orientations of the electric field(E), the magnetic field(H) and the wave vector(K) are shown in Fig. 1(b). The incident angle is 0. The boundary conditions are set as perfect electric conductor and perfect magnetic conductor on two pair faces. The dielectric permittivity of gold is modeled using the Drude model[7]:

$$\varepsilon = 1 - \frac{\omega_P^2}{\omega^2 + i\omega\gamma}. \tag{1}$$

with a plasma frequency $\omega_p = 1.37 \times 10^{16}$ rad/s and scattering frequency $\gamma = 4.08 \times 10^{13}$ rad/s.
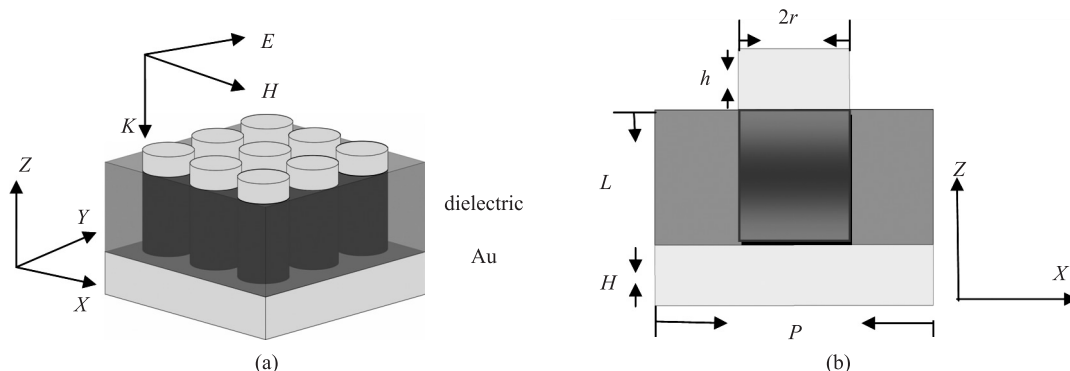

Fig. 1 (a)Schematic of the cylindrical cavity array; (b)Cross section view of the cylindrical microcavity in the $Y-Z$ plane. r, h, L and P represent gold disk radius, thickness of gold disk, height of the microcavity and period, respectively

2 Results and Discussion

In order to study the resonant characteristics of cylindrical microcavity, we calculate the reflectivity spectra $R(\omega) = |S_{11}(\omega)|^2$ at normal incident TM plane wave. As shown in Fig. 2, the resonant cavity mode appears as a reflection dip in the spectra. Moreover, the grating period is kept subwavelength, so that the only contribution in the
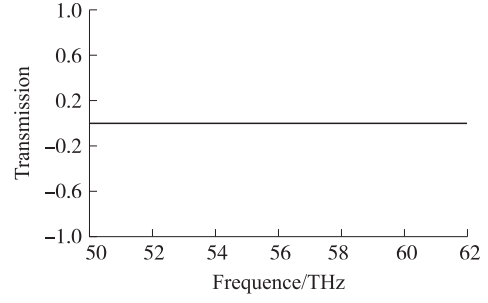
reflected signal is the specular reflection (0th diffraction order)[6]. We also calculate the transmission of the structure shown in Fig. 1, and obtain near zero transmission for all geometry parameters, as shown in Fig. 2. According to the equation:
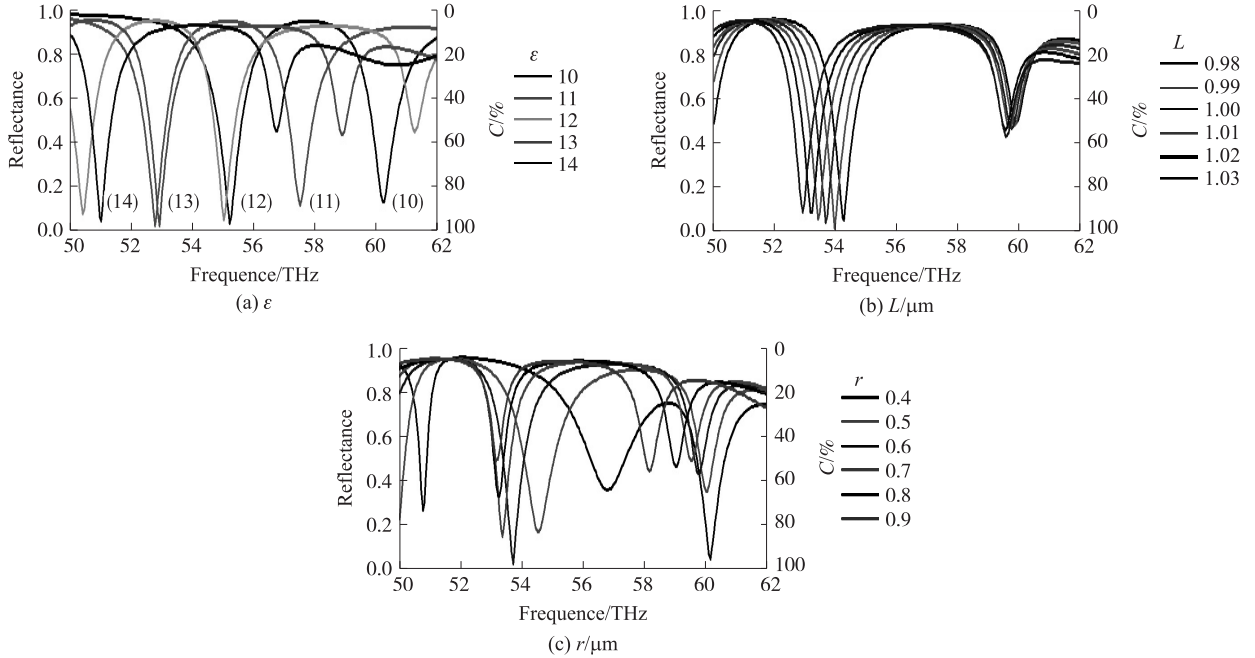
$$T+R+C=1. \tag{2}$$

Here, T, R and C represent transmission, reflection and absorption, respectively. Due to $T=0$, the minimum of reflection appears as the maximum of absorption. If we define $C=1-R_{min}$, where R_{min} is the reflectivity minimum at the resonant frequency, a larger C indicates a stronger absorption efficiency.

Fig. 2 Transmission spectra of the cylindrical microcavity in the MDM structure at normal incident TM plane wave

2.1 High absorption characteristic

Fig. 3(a) is the reflectivity spectra of the cylindrical microcavity in the MDM structure at normal incident with variable dielectric constant ε, here $L=1$ μm, $h=0.45$ μm, $H=0.45$ μm, and $P=3$ μm. When ε is changed from 10 to 14(with a step of 1), the resonant frequency is around 60.3 THz, 57.5 THz, 54.95 THz, 52.9 THz, and 51 THz, and C is 85%, 88%, 97%, 99%, 97%, respectively. It can be seen that the reflection peaks show red-shift with the increasing of the dielectric constant, and this means that the greater the dielectric constant is, the greater the near-field couples. This is because the change of the effective dielectric permittivity [$\varepsilon(\omega)$] of the system results in a shift of the electric resonance frequency. And the rate of red-shift is proportional to the dielectric constant. Ref.[8] gets the same conclusion, but it only provides absorption peaks of two different dielectric constants. Fig. 3(a) systematically gives five absorption peaks, when ε is changed from 10 to 14(with a step of 1). They provide more valuable reference to the optimization of the cylindrical cavity. Fig. 3(b) shows the reflectivity spectra as a function of L. As shown in Fig. 3(b), the resonant frequency mainly locates in the range of 53.7 ± 0.75 THz, whose dependence on L is relatively weak[8]. In contrast, the dielectric constant ε has much more greater impact on the electric dipole resonances due to the exciting of external electric field than L. At $L=0.98$ μm, C is 96%. When L is increased to 0.99 μm, C reaches maximum:99%. A further increase in L will reduce C. At $L=1.00$ μm, C declines

(a) ε

(b) L/μm

(c) r/μm

Fig. 3 Reflection spectra of the cylindrical microcavity in the MDM structure at normal incident TM plane wave

(a) Reflectivity spectra with the change of dielectric constant ε, $L=1$ μm, $h=0.45$ μm, $H=0.45$ μm, $P=3$ μm. (b) Reflection spectra with the change of L, $r=0.6$ μm, $H=0.45$ μm, $P=3$ μm. (c) Reflectivity spectra with the change of r, $L=1$ μm, $h=0.45$ μm, $H=0.45$ μm, $P=3$ μm

to 98%. When L changes from 1.01 μm to 1.03 μm, absorption efficiency inside cavity continues to fall. The results show that the absorption efficiency inside cavity is closely related to L. Fig. 3(c) presents reflectivity spectra as a function of r, here $L=1$ μm, $h=0.45$ μm, $H=0.45$ μm, $P=3$ μm. When r increases from 0.4 μm to 0.9 μm(with a step of 0.1 μm), the resonant frequency locates at 56.25 THz, 54.25 THz, 53.7 THz, 53.35 THz, 53.2 THz, and 53.15 THz respectively and C equals to 71%, 89%, 99%, 88%, 69%, and 50% respectively. As shown in Fig. 3(c), the resonant peaks show red-shift with the increasing of radius, which has similar trend as Fig. 3(a), and this near-field coupling phenomenon has been reported in Ref.[6]. The results also show that the absorption efficiency inside cavity is sensitive to the radius of gold disk.

2.2 Strong confinement features

As reported in the Ref.[6], the energy of incidence wave is dissipated by both the metallic and the dielectric loss and the large part of the energy can been localized in the dielectric microcavity. In order to study the regularity of the energy density in the condition of different parameters, we calculate the energy density of the electromagnetic field inside the cylindrical cavity with the change of the dielectric constant, the thickness of the dielectric slab and the radius of gold disk. Because of energy conservation, the peak electrical energy is equal to the average total energy inside the cavity, and the solution is achieved by integrating $E \cdot E^*$ within the volume:

$$E_d = \int_V \frac{E \cdot E^*}{V} \mathrm{d}v. \tag{3}$$

Here V is volume of the cavity, E_d is the average energy density inside the cavity, E represents the electric field vector inside the cavity. First, we calculate the energy density E_{d1} inside the dielectric cavity in the MDM structure. Then, we calculate the energy density E_{d2} inside the vacuum cavity without the MDM structure, whose shape and size are same with the dielectric cavity. We define $G=E_{d1}/E_{d2}$ as the enhancement factor of energy density. A cavity with too big or small volume will affect the EM energy absorption and confinement inside the cavity[4]. Only when parameters of material and geometry are optimized and the impedance of the structure matches the impedance of vacuum, will the extreme confinement of EM field and strong absorption inside cavities appear. Fig. 4(a) shows the enhancement factor of energy density G as a function of ε. It can be seen that the enhancement factor G increases with the increase of the dielectric constant ε. Due to the near-field coupling between the top and bottom metal layer become stronger[8], the ability of localizing the light inside the dielectric cavities is strengthened as shown in Fig. 4(a). Fig. 4(b) shows energy density ratio G as a function of the thickness of the dielectric slab L. As shown in Fig. 4(b), when L is changed from 0.98 to 0.99 μm, G shows the trend of growth. When L is increased to 0.99 μm, G reaches maximum 4 180. A further increase in L will reduce G. At $L=1.03$ μm, G declines to 2 945. The Fig. 4(b) reveals very important field spreading in the plane of the metallic strip[4] when L is changed from 0.99 to 0.98 μm. So the enhancement factor G is sensitive to L and the most optimal G should also be related the effective dielectric permittivity[$\varepsilon(\omega)$] of the system.
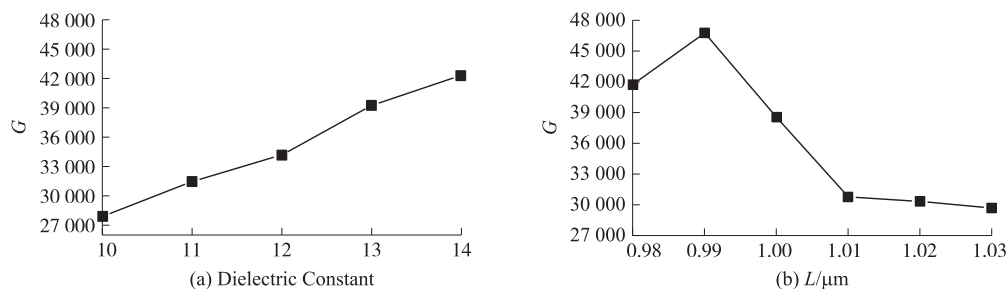

Fig. 4　(a) Energy density ratio G as a function of the dielectric constant ε;
(b) energy density ratio G as a function of the thickness of the dielectric slab L

Fig. 5(a) and Fig. 5(b) present the energy density ratio G and absorption efficiency C as a function of the radius of gold disk r, respectively. From the Fig. 5(a), we can see that G shows the trend of increase firstly and when $r=0.5$ μm, G reaches the maximum: 3 314. Afterwards, G begins to decrease. As shown in Fig. 5(b), their

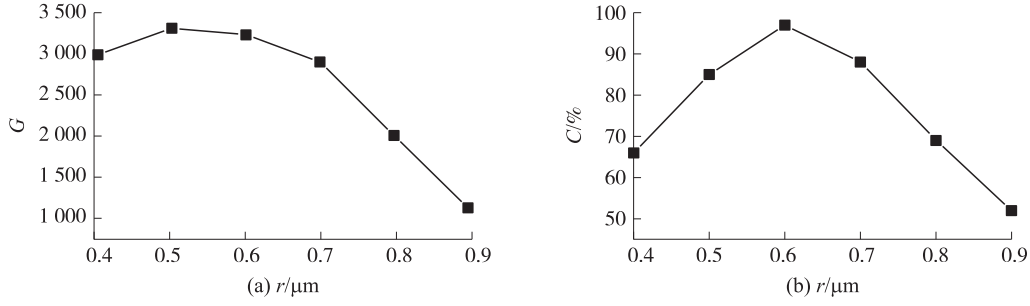**Fig. 5**　（a）energy density ratio *G* as a function of the radius of gold disk *r*（b）absorption efficiency *C*
as a function of the radius of gold disk *r*

variation trend is same as Fig. 5（a）. Their difference is that *C* reaches maximum 97% when *r*=0.6 μm. It can be seen that the maximum of *C* does not indicate the maximum of the energy density ratio. To explain this phenomenon, we use the following model（4）：

$$\frac{\varepsilon|E_{Z0}|^2}{|E_{in}|^2}=\frac{\lambda_{res}\Sigma}{2\pi V}Q_{ohm}C\cos\theta,\tag{4}$$

where ε is the dielectric constant of the middle layer, $V=\pi r^2 L$ is the volume of the cylindrical resonator, E_{in} is the electric field amplitude of the incoming wave, E_{Z0} is the amplitude of the mode resonantly excited in the microcavity and θ is the incident angle. For the data reported here we have $\cos\theta=1, \Sigma=P^2, Q_{ohm}$ is the quality factor Q of the Ohmic loss. When $r=0.6$ μm, $C=0.97$ and G is 3 232; At $r=0.5$ μm and $R=3$ 314, C is 0.85. Because Q_{ohm} approximately equals in the bands studied here we can get $\dfrac{\varepsilon|E_{Z0}|^2}{|E_{in}|^2}\sim\lambda_{res}C/V$, indicating that the energy density ratio inside the cavity is decided by $\lambda_{res}C/V$. At $r=0.6$ μm, its $\lambda_{res}C$ is greater than that at $r=0.5$ μm. As the volume plays the most important role in R, R reaches the maximum（3 314）at $r=0.5$ μm.

2.3　Physical mechanism

To explore the physical mechanism of the extreme confinement and perfect absorption inside cavity, the distributions of the EM field intensity and current at the resonant mode（$f=53.7$ THz）are simulated, as shown in Fig. 6. Fig. 6（a）shows the amplitude of electric field at the middle of the dielectric layer in the $X-Y$ plane. The gray circle represents the cylindrical microcavity. A standing wave pattern is clearly shown in Fig. 6（a）.The amplitude of the electric field can be approximated by the expressions：

$$|E|\sim\cos\frac{\pi X}{\Delta x}(0\leqslant X<r).\tag{5}$$

At $r=0$, $|E|$ reaches its maximum, that is, energy is strongly localized around the center of the cylindrical microcavity. Fig. 6（b）presents the amplitude of electric field at the middle of the dielectric layer in the $Y-Z$ plane. In this figure, the white area represents the metal, the middle layer is dielectric and the EM field is highly localized between the two metal layers, which can be approximated as a standing wave too. The confining mechanism, which arises from the impedance mismatch between the metal-metal and single metal regions[5], is responsible for the formation of the standing wave patterns. The perfect absorbing characteristics may be explained by Fig. 6（c-e）. Fig. 6（c）shows amplitude of electric field on the top surface of the dielectric layer, here the gray circle represents the position of gold disk. As indicated in Fig. 6（c）, the distribution of electric field mainly concentrates around the gold disk, forming a square area. However, the amplitude of electric field in the center of gold disk is weaker than that in the surrounding. Meanwhile, it can be seen clearly that six"hot spots"symmetrically locate in the four edges of the square area and both sides of the gold disk in the Y-axis direction. In this case, gold disk can be regarded as the electric dipole resonator by the external electric field excitation. A change in the disk diameter will result in a shift of the electric resonance frequency, and hence result in a change of the effective dielectric permittivity[$\varepsilon(\omega)$] of the system. Fig. 6（d）is the distribution of the current at the middle of the dielectric layer in the $Y-Z$ plane.The white areas in this figure are the two metal layers. The magnetic field distribution shown in Fig. 6（d）clearly indicates the localization of magnetic field between two metal layers, thus the forming of the magnetic dipole resonance.

A change in the dielectric layer thickness mainly affects the magnetic resonance and the effective magnetic permeability $[\mu(\omega)]$ of the system. By optimizing the parameters of the top gold layer and dielectric layer thickness, we can tune ω of the ε and μ resonances. When we achieved $\varepsilon = \mu (Z = \sqrt{\dfrac{\varepsilon(\omega)}{\mu(\omega)}} = 1)$ and thus an impedance near the free space value. While strongly coupling the incident radiation to the resonant structure and perfect absorbance is theoretically possible, it can only occur when the MM layer is impedance-matched to free space[9].
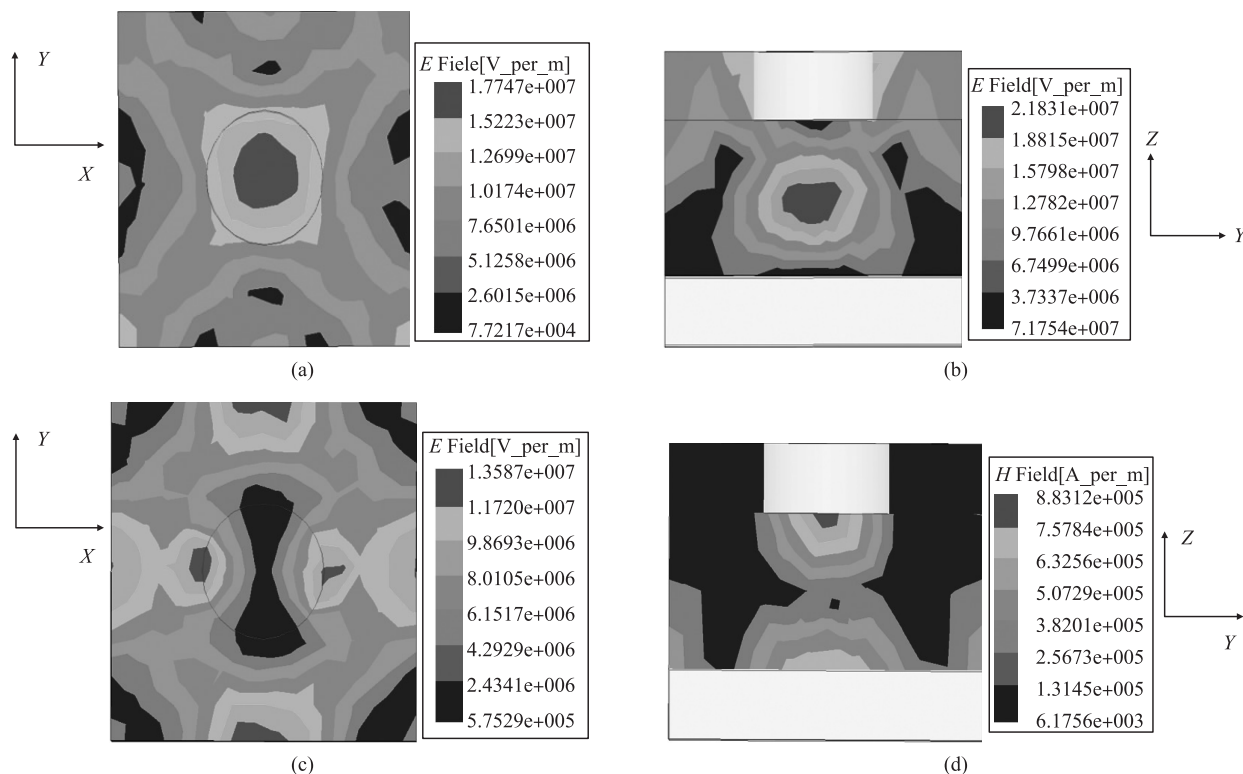

Fig. 6 Distributions of EM field intensity and current within cylindrical cavities at normal incident TM plane wave

(a) Amplitude of electric field at the middle of the dielectric layer in the $X-Y$ plane at $f = 53.7$ THz; (b) Amplitude of electric field at the middle of the dielectric layer in the $Y-Z$ plane at $f = 53.7$ THz; (c) Amplitude of electric field on the top surface of the dielectric layer at $f = 53.7$ THz; (d) Amplitude of magnetic field at the middle of the dielectric layer in the $Y-Z$ plane at $f = 53.7$ THz.

3   Conclusions

We have numerically studied the electromagnetic energy density and absorption efficiency inside the MDM cylindrical microcavities in the mid-infrared range. With the change of the thickness of the dielectric slab, dielectric constant and the radius of gold disk, the G and C present some important regularity for us to modulate resonance frequency and strengthen electromagnetic energy density. The enhancement factor G increases with the increase of the dielectric constant ε. When L is changed from 0.98 μm to 1.03 μm, G increases firstly, and then decreases. When $L = 0.99$ μm, G reaches maximum 4 180. At $L = 1$ μm, $H = 0.45$ μm, $h = 0.45$ μm and $r = 0.6$ μm, C is 0.97 and R is 3 232. When $r = 0.5$ μm, other conditions unchanging, C is 0.85 and R is 3 314. It can be seen that the maximum of C does not indicate the maximum of the energy density ratio. This kind of strong absorption and high localization make the proposed structures have broad applications in areas such as surface enhanced spectroscopy, new plasmonic detectors, bio-sensing, solar cells, and so on.

[参考文献]

[1]   DU L P, ZHANG X J, MEI T, et al. Localized surface plasmons, surface plasmon polaritons and their coupling in 2D metallic array for SERS[J]. Opt Express, 2010, 18:1 959-1 965.

[2]   MAIER S A, ATWATER H A. Plasmonics:localization and guiding of electromagnetic energy in metal/dielectric structures[J].

J Appl Phys,2005,98:011101-1-011101-10.

[3] KOGELBAUER I,HEINE E. Adaptation of soil physical measurement techniques for the delineation of mud and lakebed sediments at neusiedler see[J]. Sensors,2013,13:17 067-17 083.

[4] FEVILLET P C,TODOROV Y,STEED R. Extremely sub-wavelength THz metal-dielectric wire microcavities[J]. Opt Express, 2012,20:29 121-29 130.

[5] TODOROV Y,TOSETTO L,TEISSIER J,et al. Optical properties of metal-dielectric-metal microcavities in the THz frequency range[J]. Opt Express,2010, 18:13 886-13 907.

[6] FEVILLET P C,TODOROW Y,VASANELLI A,et al. Strong near field enhancement in THz nano-antenna arrays[J]. Sientific reports,2013(3):299-308.

[7] WANG X D,YE Y H,ZHANG C. Tunable figure of merit for a negative-index metamaterial with a sandwich configuration[J]. Opt Lett,2009,34:3 568-3 570.

[8] CHEN K,WEN Q Y,ZHANG H B. Study on the broadband terahertz metamaterial absorber[J]. Electronic components and materials,2011,30:56-59.

[9] LANDY N I,SAJUYIGBE S. Perfect metamaterial absorber[J]. Physical Review Letters,2008,100:1 586-1 594.

[责任编辑:顾晓天]

[15] LEE S,LI L,WANG Z,et al. Immersed transparent microsphere magnifying sub-diffraction-limited objects[J]. Applied optics, 2013,52(30):7 265-7 270.

[16] HAO X. LIU X,KUANG C,et al. Far-field super-resolution imaging using near-field illumination by micro-fiber[J]. Applied physics letters,2013,102(1):1-4.

[17] HAO X,KUANG C,. LI Y,et al. Evanescent-wave-induced frequency shift for optical superresolution imaging[J]. Optics letters,2013,38(14):2 455-2 458.

[18] HAO X,KUANG C,GU Z,Y,et al. From microscopy to nanoscopy via visible light[J]. Light-science and application,2013,10 (e108):1-10.

[责任编辑:顾晓天]